

4 Photodissociation of CSCI₂ at 235 nm: Kinetic Energy Distributions and Branching Ratios of Cl Atoms and CSCI Radicals

The photodissociation dynamics of thiophosgene (CSCI₂) and the respective branching ratios of both dissociation products Cl and CSCI have been studied by 3D imaging of the photodissociation product chlorine in its ground state ²P_{3/2} [Cl] and excited spin-orbit state ²P_{1/2} [Cl*] employing the resonance enhanced multi-photon ionization and time-of-flight technique (REMPI-TOF) at a dissociation wavelength of about 235 nm. A novel technique is applied where the complete three-dimensional (3D) momentum vector of a reaction product is directly determined. The kinetic energy distribution (KED) for Cl* is observed for the first time. The obtained KEDs of Cl and Cl* are different in the low kinetic energy range due to the correlating state of the partner fragment CSCI. In the case of ground state Cl the CSCI partner radical is produced in the ground state \tilde{X} , in the \tilde{A} and \tilde{B} states with a contribution of 4 ± 0.5 %, 60 ± 5 %, and 36 ± 3 %, respectively. In the case of Cl* the corresponding CSCI is produced with a contribution of 7.5 ± 0.5 % in the ground state \tilde{X} , 71.5 ± 5.5 % in the state \tilde{A} , and 21 ± 1.5 % in the state \tilde{B} . The yield of Cl*, $\phi(\text{Cl}^*) = P(\text{Cl}^*) / [P(\text{Cl}) + P(\text{Cl}^*)]$, was found to be 0.47. No significant velocity dependence of the anisotropy parameter β could be observed. The mean value of 0.03 suggests a decay on the \tilde{B} (A₁) surface.

4.1 Introduction

The implication of a novel 3D imaging technique that allows to monitor the full 3D momentum vectors of individual products of a chemical elementary reaction¹ has led to a detailed examination of the ultraviolet photodissociation of a series of tetratomic star-like molecules^{2,3} which can, in principle, decay into three fragments. Adequate projection methods allow to extract state-specific fragment kinetic energy distributions as well as the anisotropy parameter β describing the spatial fragment distribution from the 3D momentum data. Especially the determination of the velocity dependence of the anisotropy parameter proved to be useful in the analysis of competing two- and three-body channels in

the photodissociation of SOCl₂^{2,4} and COCl₂^{3,5}. We present here a study of the structurally similar thiophosgene (CSCI₂) molecule which offers the possibility to investigate a different electronic transition than in the phosgene case at the same dissociation energy.

Thiophosgene, CSCI₂, has been the object of extensive studies both in the gas phase and in solution because it offers insight into several important aspects of electronic spectroscopy, photophysics, and photochemistry.⁶⁻¹⁶ One advantage of thiophosgene is its thermal stability and ready availability. The structure of its ground state (\tilde{X}^1A_1) in C_{2v} symmetry is well known.¹⁷ The electron configuration of the ground state has been determined by photoelectron spectroscopy to be

$$[\text{core}] (9a_1)^2(10a_1)^2(6b_1)^2(11a_1)^2(7b_1)^2(3b_2)^2(12a_1)^2(2a_1)^2(8b_1)^2(13a_1)^2(4b_2)^2(9b_1)^2,$$

where the 9a₁, 6b₁, and 10a₁ molecular orbitals (MOs) contain the σ bonding electrons, the 3b₂ MO contains the π bonding electrons, and the 9b₁ and 13a₁ MOs contain the sulfur lone pair electrons.¹⁸ The thiophosgene absorption spectrum as shown in Fig. 4.1 was reported by Farnworth and King.¹⁹

Thiophosgene absorbs weakly in the visible region to produce the lowest triplet and lowest excited singlet states, T₁ (\tilde{a}^3A_2) and S₁ (\tilde{A}^1A_2), respectively, which corresponds to a symmetry-forbidden $\pi_{CS}^* \leftarrow n_S$ (5b₂ \leftarrow 9b₁) electron promotion. Illumination in the strong band system in the near-UV region populates the second excited singlet state, S₂ (\tilde{B}^1A_1), which arises from the allowed promotion of a 4b₂ electron to the 5b₂ MO. The $\tilde{B}^1A_1 \leftarrow \tilde{X}^1A_1$ transition is therefore $\pi_{CS}^* \leftarrow \pi_{CS}$ in character, and results in lowering the C-S bond order from 2 to 1, lengthening the equilibrium C-S bond length by about 0.5 Å, and decreasing of the Cl-Cl bond angle from 111.2° to 103.0°.²⁰ Farnworth and King's analysis¹⁹ indicated that the molecule is non-planar in the upper ¹A₁ state with an out-of-plane angle of 20° and an inversion barrier of 126 cm⁻¹. Studies of the gas-phase photochemistry^{14,15} and photophysics²¹ of thiophosgene have flourished since the discoveries of fluorescence from both the S₁ (\tilde{A}^1A_2) and S₂ (\tilde{B}^1A_1) states.^{22,23} The fluorescence from the first singlet S₁ and the second singlet S₂ has been observed at wavelengths above 455 nm^{23,24} and 277 nm,^{22,23} respectively. The spectrum in the 240 nm to 287.5 nm region shows no fine structure and only the vibrational structure is apparent down to 268 nm.¹⁹

Below this wavelength the bands become very diffuse, indicating increasing predissociation of the upper state within 10^{-13} s.¹⁴

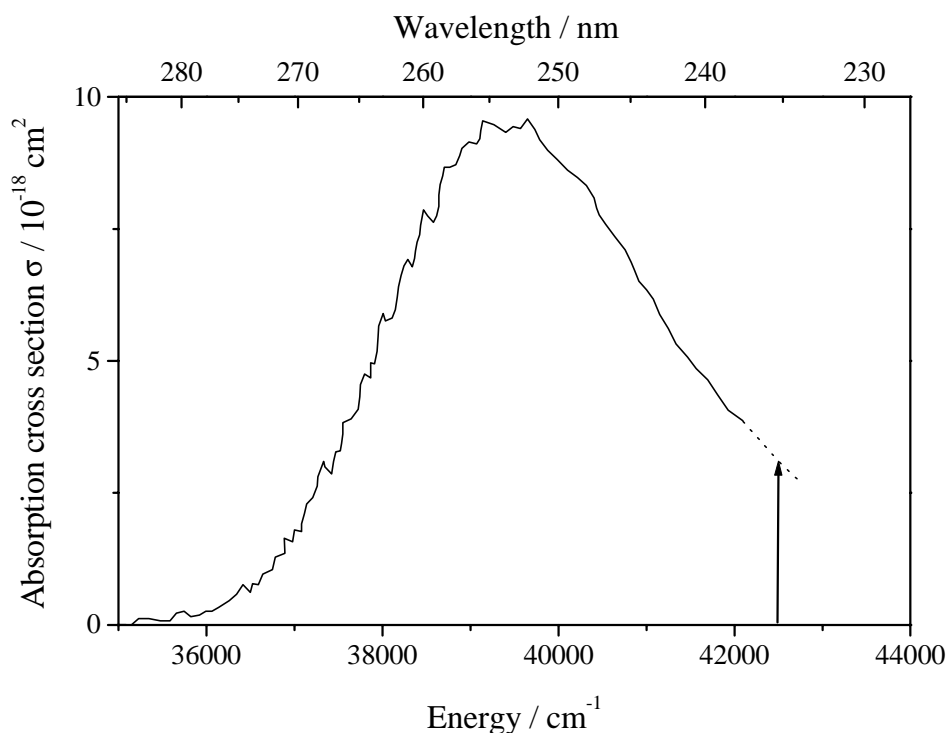


Figure 4.1: Absorption cross section of CSCI₂ based on the publication of Farnworth and King (ref. 19). The wavelength used in the present experiment is marked by an arrow. Due to the lack of experimental data in the present wavelength region, the absorption cross section is extrapolated.

Excitation at higher energies (e.g. $\lambda = 248$ nm) does not produce observable fluorescence, but results exclusively in photodissociation. The mechanism of the photodissociation of this tetraatomic molecule can be characterized by three possible decay mechanisms. For the photodissociation of CSCI₂ above 200 nm, the radical (4.1) and the molecular channel (4.2) produce two fragments:



Below 221 nm the excitation energy exceeds the energy required to break both Cl-C bonds, and three-body dissociation²⁵ (4.3) may also take place:



Other than in phosgene, excitation at 235 nm will not access the lowest $^1\text{A}_2$ state, but the second absorption band associated with the $^1\text{A}_1$ state. The absorption cross-section is much stronger ($\sigma_{235}(\text{CSCI}_2) = 4 \cdot 10^{-18} \text{ cm}^{-1}$, $\sigma_{235}(\text{COCl}_2) = 9 \cdot 10^{-20} \text{ cm}^{-1}$) because contrary to COCl_2 the CSCI_2 transition is symmetry-allowed. The wavelength shift in the absorption spectrum is due to the substitution of the oxygen atom by a sulfur atom. The relative weakness of the C-S bond goes along with a strengthening of the C-Cl bond, and the three-body threshold is increased such that the three-body channel (4.3) is not accessible at a dissociation wavelength of 235 nm. Thus, a similar situation is created as in the photodissociation of COFCl where the substitution of a chlorine by a fluorine atom also closes the three-body decay channel.²⁶ Contrarily to the case encountered here, the accessed state for COFCl was the same $^1\text{A}_2$ state as in phosgene so that by chemical substitution the first step of a three-body break-up could individually be studied.

CSCI and Cl_2 fragments were detected from 248 nm laser photolysis of a pulsed molecular beam of CSCI_2 .¹⁵ These fragments formed under collision free conditions were explained by two decomposition pathways: reaction (4.1) and (4.2). The quantum yield for (4.1) was found to be 0.8 ± 0.1 and the experimental energy release E_T/E_{av} 0.29 ± 0.01 , where E_T is the averaged total translational energy and E_{av} the maximal energy available to the fragments after dissociation. The observed translational energy release was only in modest agreement with the calculated value of 0.37 which was predicted by employing the impulsive spectator model.²⁷ This deviation led Hachey et al.¹⁶ to question, whether the original assumption that CSCI was produced exclusively in its bent electronic ground state was correct. Calculations by Chan and Goddard²⁸ and by Hachey et al.¹⁶ showed that a very low lying excited singlet linear state is thermodynamically accessible. Hachey et al. reevaluated via ab initio CI studies the geometry of the ground and the first electronically excited states of the CSCI radical, the vertical excitation energies of its ten lowest doublet states and two lowest quartet states to construct a more complete energy level correlation diagram. These studies show that the three possible states $\tilde{\text{X}}$, $\tilde{\text{A}}$, and $\tilde{\text{B}}$ of the CSCI fragment can be accessed in the UV photofragmentation of CSCI_2 which are already introduced in the reaction scheme of the radical decay channel (4.1).

Despite this, the question about their relative importance has not yet been answered. In the present work the photofragmentation dynamics of CSCI₂ are studied when irradiated around 235 nm. The purpose of the present work is to determine (i) the complete 3D velocity distribution for both ground state Cl and excited state Cl* and the respective anisotropy parameter β , (ii) the contribution of the \tilde{X} , \tilde{A} and \tilde{B} states of CSCI, and (iii) the spin-orbit branching ratio of Cl*/Cl.

4.2 Experiment

A more detailed description of the experimental set-up and the novel position-sensitive detector (PSD) has been published elsewhere.^{1,3} Briefly, it consists of a combination of a home-built single-field time-of-flight (TOF) mass-spectrometer and a position-sensitive detector.²⁹⁻³¹ The spectrometer was evacuated to a base pressure of about 10^{-8} mbar by a turbo molecular pump system. Thiophosgene was constantly cooled to -20°C to prepare a mixture of about 0.5 % CSCI₂ in helium. The mixture was fed into the spectrometer via a continuous supersonic beam. With a nozzle diameter of 20 μm and a stagnation pressure of about 3 bar typical working pressures were in the order of 10^{-7} mbar. Under these conditions the beam is characterized by a rotational temperature of about 8 K, determined by a rotationally resolved calibration spectrum of the NO ($A^2\Sigma^+ \leftarrow X^2\Pi$) transition.¹

Simultaneous dissociation and state-selective detection of chlorine atoms were performed using one dye laser pumped by a Nd:YAG laser (Coherent, Infinity 40 100). The dye laser (Lamba Physik, Scanmate) was operated with Coumarin 47 at a repetition rate of 100 Hz, its light was frequency-doubled by a BBO crystal and focussed by a 20 cm lens in order to decrease the reaction volume to $5 \cdot 10^{-4}$ mm³. The energy of the frequency-doubled light was kept low (< 1 μJ) to obtain approximately one fragment signal per ten laser pulses to avoid kinetic energy transfer to the fragments due to space charge effects and saturation of the dissociation step. The laser beam, the molecular beam, and the detector axes were mutually orthogonal in the interaction region. Ultimate care was taken to overlap the light and the molecular beam which was checked frequently by monitoring of NO via (1+1) REMPI at 226 nm and optimizing the signal intensity.³² The polarization of the laser was changed by a half wave plate in order to investigate the spatial fragment distribution. Typically the

acceleration voltage was 800 V in the acceleration tube of the TOF spectrometer corresponding to an acceleration field of 16 kV/m.

The 2P_J state of the chlorine atom is split by 882 cm^{-1} due to spin orbit-coupling into $\text{Cl}(^2P_{3/2})$ and $\text{Cl}^*(^2P_{1/2})$. Both states were detected by a (2+1) REMPI process. The ground state was probed via the ($^2D_{3/2} \leftarrow ^2P_{3/2}$) transition at 235.336 nm, the excited state by the ($^2P_{1/2} \leftarrow ^2P_{1/2}$) transition at 235.205 nm. Typically the dye laser was scanned over a range of ± 0.003 nm around the center transitions accounting for the Doppler broadening. Signals were digitized by time-to-digital converters (TDCs), accumulated over $2 \cdot 10^5$ laser shots, and saved on-line by a personal computer. The analyzing procedure is described in detail elsewhere.³

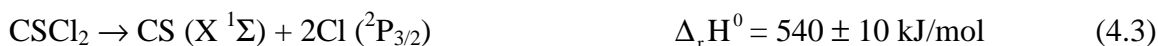
The PSD includes a delay-line anode (DLA) introduced into the spectrometer chamber right behind the double stage micro-channel plates (MCPs). The PSD allows us to monitor all three components of the momentum vector from the measured position of one particle on the detector and its corresponding time-of-flight (TOF). Therefore, a full 3D velocity distribution is observed and the complete information about the kinetic energy distribution and the velocity dependent anisotropy parameter β can be extracted.

4.3 Results and Discussion

The $\tilde{B}(^1A_1) - \tilde{X}(^1A_1)$ band system of CSCI₂ molecules has been extensively studied by spectroscopists^{8,9,16,33} who found out that the onset of predissociation required 427.4 ± 0.6 kJ/mol, i.e. 17.3 ± 0.6 kJ/mol above the $\tilde{B}(^1A_1)$ state.

Reaction enthalpies $\Delta_r H$ for the three photodissociation channels of CSCI₂ are calculated from the enthalpies of formation $\Delta_f H$ of the reactants:





There are some uncertainties in the enthalpies of formation $\Delta_r H^0$ for the CSCI₂ and CSCl molecules. For this study, the $\Delta_r H^0$ of the CS radical was adopted from the most recent literature source.³⁴ The $\Delta_r H^0$ of CSCI₂ and CSCl ($\tilde{\text{X}}$, $\tilde{\text{A}}$, and $\tilde{\text{B}}$) were obtained from Joshi³⁵ and Hachey et al.,¹⁶ respectively. Hachey et al. based the calculation of $\Delta_r H^0$ of the different CSCl states on the publication of Okabe¹⁴, who determined the bond energy $D_{0(\text{SCCl-Cl})}$ to be 265 ± 2.5 kJ/mol. The enthalpies $\Delta_r H^0$ of the reactions above were calculated for the spin-orbit ground state Cl, so $\Delta_r H^0$ required for the generation of one Cl* atom is higher by 10.6 kJ/mol.

As the molecular channel (4.2) cannot be observed in our experiment and the three-body decay channel (4.3) is energetically not allowed at the wavelength of 235 nm, we concentrated on the details of the two-body decay channel (4.1), the spin-orbit branching ratio of Cl*/Cl and the relative importance of the different states of CSCl which are not yet established with certainty.³⁶

4.3.1 Spin-Orbit Branching Ratio Cl*/Cl

The spin-orbit branching ratio was obtained by scanning the laser over the two resonance transitions of Cl and Cl*. The measurements were repeated at different laser light intensities. Integrating the area under the Doppler profiles results in a signal ratio $S(\text{Cl}^*)/S(\text{Cl})$ of 0.80 ± 0.04 . Taking the ratio of transition probabilities B of 1.06 ³⁷ into account we determined a Cl* yield $\phi(\text{Cl}^*) = 0.47 \pm 0.03$ where ϕ is defined as the ratio of the number of excited state atoms $P(\text{Cl}^*)$ to the total number of chlorine atoms: $\phi(\text{Cl}^*) = P(\text{Cl}^*)/[P(\text{Cl})+P(\text{Cl}^*)]$. On statistical grounds one expects a yield of $\phi_{\text{statistical}} = 0.33$.

4.3.2 Fragment Kinetic Energy and Angular Distribution

In Fig. 4.2 the kinetic energy distributions (KEDs) and the anisotropy parameter β are presented for the photodissociation of thiophosgene around 235 nm for both spin-orbit states. Here β , the anisotropy parameter ranging from -1 (perpendicular transition) to $+2$ (parallel transition), characterizes the spatial fragment distribution:

$$P(\theta, v) \propto f(v)(1 + \beta(v)P_2(\cos\theta)),$$

where θ is the angle of the polarization vector of the dissociating laser with the product recoil velocity vector, and P_2 is the second Legendre polynomial: $P_2(x) = \frac{1}{2}(3x^2 - 1)$. The 1D KED presentation is obtained via integration of the 3D data, while for the anisotropy parameter β the velocity dependency is evaluated from the 3D data subdivided into velocity ranges of 200 m/s. Although both Cl and Cl* are released with kinetic energies in the whole available energy range up to the calculated limit of 170 kJ/mol, a remarkably different behavior of the two spin components with respect to their kinetic energy acquisition in the photodissociation is obvious.

The KED of ground state Cl is bimodal releasing Cl mainly with low kinetic energy, where a shoulder is obtained at intermediate energy range with a tail reaching the high energy range. In comparison the KED of excited state Cl* is broad showing no preference for very low kinetic energies. No fine structure is observed over the whole energy range. The maximal available kinetic energy of one Cl fragment is calculated from the bond energy of 265.3 kJ/mol given by Okabe¹⁴ assuming that the partner fragment SCl has no internal energy.

Chlorine is almost isotropically released: The spatial fragment distribution is characterized by very small averaged β parameters of 0.01 ± 0.05 and 0.06 ± 0.06 for Cl and Cl*, respectively. The β parameters are almost velocity independent within the experimental error, only a very small increase is observed at very high kinetic energies (see Fig. 4.2 and Table 4.1).

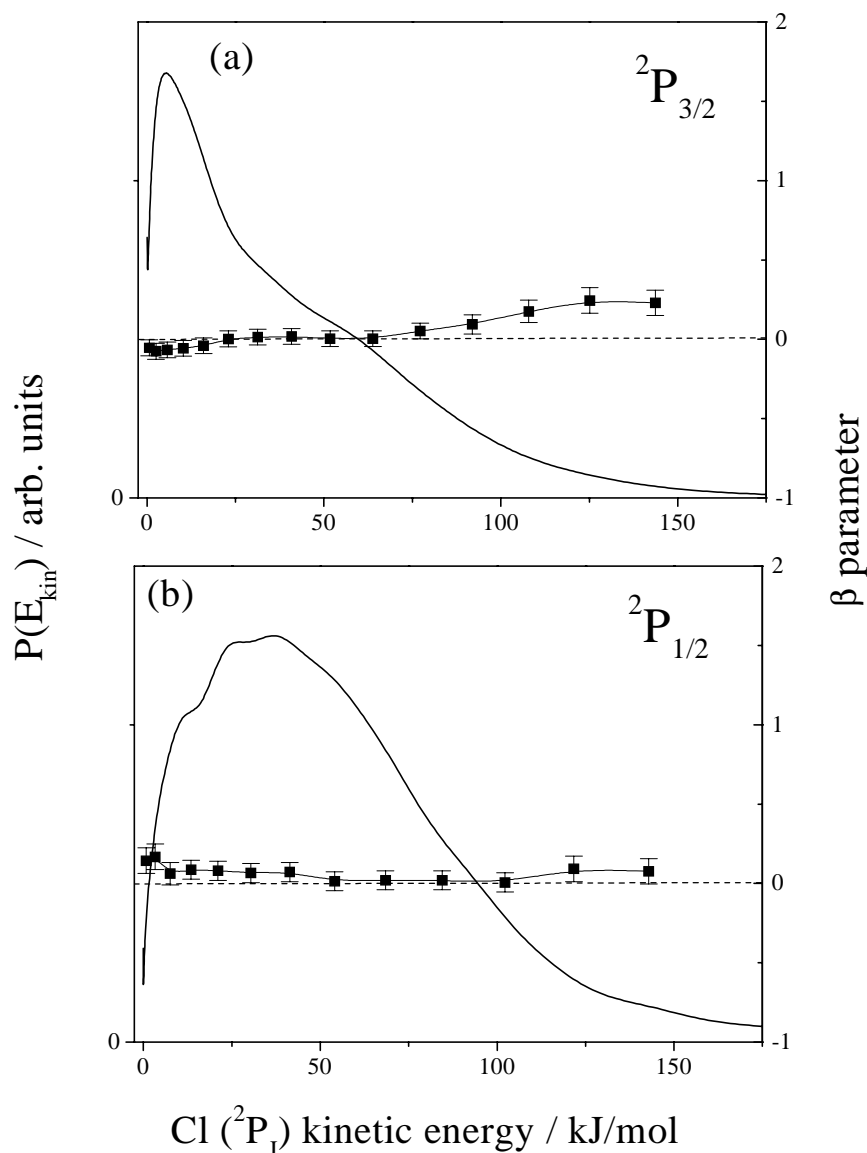


Figure 4.2: Kinetic energy distribution for (a) ground state Cl(²P_{3/2}) and (b) excited state Cl*(²P_{1/2}) atoms produced in the photodissociation of CSCI₂ at 235 nm. The dependence of the β parameter on the Cl fragment kinetic energy (right scale) is shown by curves with error bars. This 1D presentation is obtained via integration of the 3D data.

The theoretical limit for the β parameter for an instantaneous decay from the excited ¹A₁ state geometry with a Cl-C-Cl bond angle of 103° is 0.08.²⁰ The respective transition dipole moment μ is oriented along the C₂ axis containing the CS bond. Although lack of anisotropy can be due to an excited state lifetime longer than a rotational period, the geometry of the molecule and the transition moment resulting in a half bond angle between

Cl-Cl close to the magic angle $\theta_m = 54.7^\circ$ with $P_2(\cos \theta_m) = 0$, could cause an isotropic fragment distribution, even if the dissociation is direct. In agreement with Ondrey and Bersohn¹⁵ it is concluded that the dissociation proceeds directly and fast via the excited 1A_1 state of ground state symmetry.

Table 4.1: Characteristic data describing the kinetic energy distribution of Cl and Cl*, and the internal energy distribution of the partner fragment CSCI, the β parameter, the branching ratios of the CSCI fragment and the kinetic energy release $E_T/(E_{av} - E_{el})$ in the photodissociation of CSCI₂.

$$E_{av}(Cl + CSCI) = 243 \text{ kJ/mol}, E_{av}(Cl^* + CSCI) = 232.4 \text{ kJ/mol},$$

$$E_{el}(\tilde{A}) = 77 \text{ kJ/mol}, E_{el}(\tilde{B}) = 178 \text{ kJ/mol}.$$

Fragment	Correlating CSCI states	Contribution (%)	E_{int} (kJ/mol)	E_T (kJ/mol)	$E_T/(E_{av} - E_{el})$	β Parameter
Cl	(\tilde{X})	2	75	168	0.69 ± 0.04	0.20 ± 0.07
	(\tilde{A})	32	98	68	0.41 ± 0.03	0.03 ± 0.05
	(\tilde{B})	19	47	18	0.28 ± 0.03	-0.07 ± 0.06
Cl*	(\tilde{X})	3.5	57	175	0.75 ± 0.05	0.08 ± 0.07
	(\tilde{A})	33.5	77	78	0.50 ± 0.03	0.03 ± 0.06
	(\tilde{B})	10	23	31	0.57 ± 0.04	0.15 ± 0.08

4.3.3 CSCI Energy Disposal

The internal energy of CSCI is not measured directly. However, via the relation:

$$E_{int}(CSCI) = E_{av} - E_T - E_{int}(Cl) \quad (4.4)$$

$E_{int}(CSCI)$ can be determined by transforming the measured KED of both Cl and Cl* into the internal energy distribution (IED) of the respective partner fragments CSCI by conservation of linear momentum and energy according to:

$$E_T = \left(1 + \frac{m_{Cl}}{m_{CSCI}}\right) E_{kin}(Cl) \quad (4.5)$$

The available energies E_{av} in equation 4.4 is given by the photolysis energy $h\nu$ and the dissociation energy $D_{0(CSCI-Cl)}$. The internal energy of the parent molecule $E_{int}(CSCI_2)$ is negligible, yielding:

$$E_{av} = h\nu - D_{0(CSCI-Cl)} \quad (4.6)$$

The obtained IEDs via equation 4.4 are shown in Fig. 4.3 and characteristic data are summarized in Table 4.1. Three Gaussians are fitted to these internal energy distributions with respect to the calculations of the \tilde{X} , \tilde{A} , and \tilde{B} state of Hachey et al.¹⁶ Based on the Gaussian fits, the internal energies of the three electronic states can be calculated. Two aspects must be taken into account: first, the low internal energy flanks of the Gaussians reaching the energetic forbidden region must be excluded. The energetic limits are marked in Fig. 4.3 by a dotted line for the \tilde{A} and by a dashed line for the \tilde{B} state of CSCI. This energetic restriction has only a minor effect on the calculated internal energies of CSCI(\tilde{X}), CSCI(\tilde{A}), and CSCI(\tilde{B}). Secondly, the maximal energy of 243 kJ/mol limits the Gaussians at high energies. This influences essentially the contribution of CSCI(\tilde{B}).

The total internal E_{int} (including the electronic energy of the \tilde{A} and \tilde{B} state) is accordingly calculated to be 225, 175, and 75 kJ/mol which are assigned to CSCI(\tilde{B})+Cl, CSCI(\tilde{A})+Cl, and CSCI(\tilde{X})+Cl, respectively, and 201, 154, and 57 kJ/mol for CSCI(\tilde{B})+Cl*, CSCI(\tilde{A})+Cl*, and CSCI(\tilde{X})+Cl*. Considering the electronic energy E_{el} of 77 kJ/mol for the \tilde{A} state and 178 kJ/mol for the \tilde{B} state of the CSCI, one obtains for the Cl(²P_{3/2}) channel an internal energy release of 75 kJ/mol for CSCI(\tilde{X}), 98 kJ/mol for CSCI(\tilde{A}), and 47 kJ/mol for CSCI(\tilde{B}). For the Cl* channel one obtains the respective values of 57, 77, and 23 kJ/mol.

In addition, the state specific kinetic energy release $\langle E_T \rangle / (E_{av} - E_{el})$ can be calculated. Since the state specific E_T is obtained via E_{int} resulting in $E_T = 168, 68, \text{ and } 18$ kJ/mol for reactions 4.1a, 4.1b, and 4.1c, respectively, releasing ground state Cl, the total kinetic

energy release $\langle E_T \rangle / (E_{av} - E_{el})$ is evaluated to be 0.69 ± 0.04 , 0.41 ± 0.03 , and 0.28 ± 0.03 for CSCI(\tilde{X})+Cl, CSCI(\tilde{A})+Cl, and CSCI(\tilde{B})+Cl, respectively. In the case of excited state Cl* the energy release $\langle E_T \rangle / (E_{av} - E_{el})$ is 0.75 ± 0.05 , 0.50 ± 0.03 , and 0.57 ± 0.04 , where E_T is 175, 78, and 31 kJ/mol for CSCI(\tilde{X})+Cl*, CSCI(\tilde{A})+Cl*, and CSCI(\tilde{B})+Cl*. The obtained energy releases are summarized in Table 4.1.

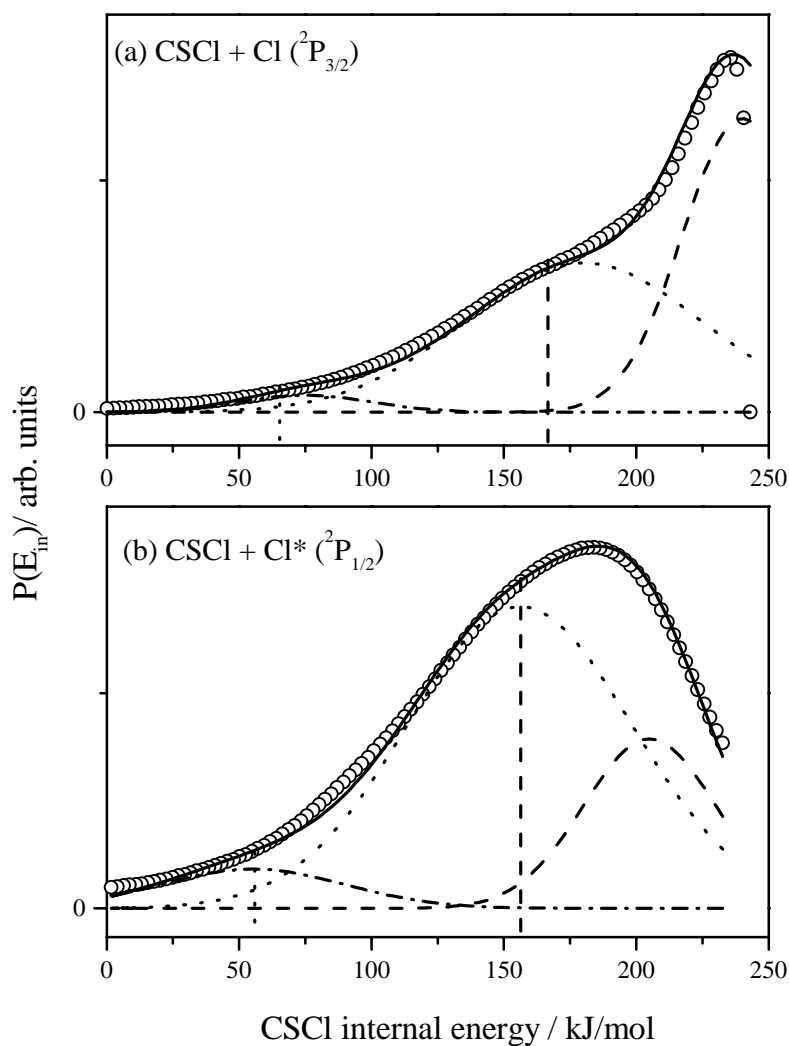


Figure 4.3: Internal energy distribution of CSCI for both (a) ground state Cl and (b) excited state Cl* partner fragments. The energetic limits taken from Hachey et al.¹¹ are marked by a dotted and a dashed line for the \tilde{A} and \tilde{B} state of CSCI, respectively. Remarkable is the different curve shape especially in the high internal energy region. Three Gaussians are fitted to the distribution in order to evaluate the contributions of the different electronic states of CSCI. The dashed line is assigned to the \tilde{B} state, the dotted line to the \tilde{A} state, and the dot dashed line to the \tilde{X} state.

It is concluded that the simple impulsive spectator model³⁸ predicting a value of $\langle E_T \rangle / E_{av} = 0.369$ can not be used for describing the photodissociation of CSCI₂ at about 235 nm in detail. This conclusion is supported by the geometry change by exciting CSCI₂ from its ground state $\tilde{X} (^1A_1)$ to its excited state $\tilde{B} (^1A_1)$ being evidence of a strong gradient of the upper potential energy surface with respect to the angle γ describing the out-of-plane bending of CSCI₂ compared to the planar ground state geometry.³⁹

4.3.4 Spin Correlation of the CSCI Partner Fragment

The obtained internal energy distributions for the partner fragment CSCI of the ground and excited state Cl atoms, shown in Fig. 4.3, allow us to study the contribution of the involved states CSCI(\tilde{X}), CSCI(\tilde{A}), and CSCI(\tilde{B}), calculated by Chan and Goddard²⁸ and Hachey et al.^{6,16} Fig. 4.4 shows the energy values¹⁶ for our present study.

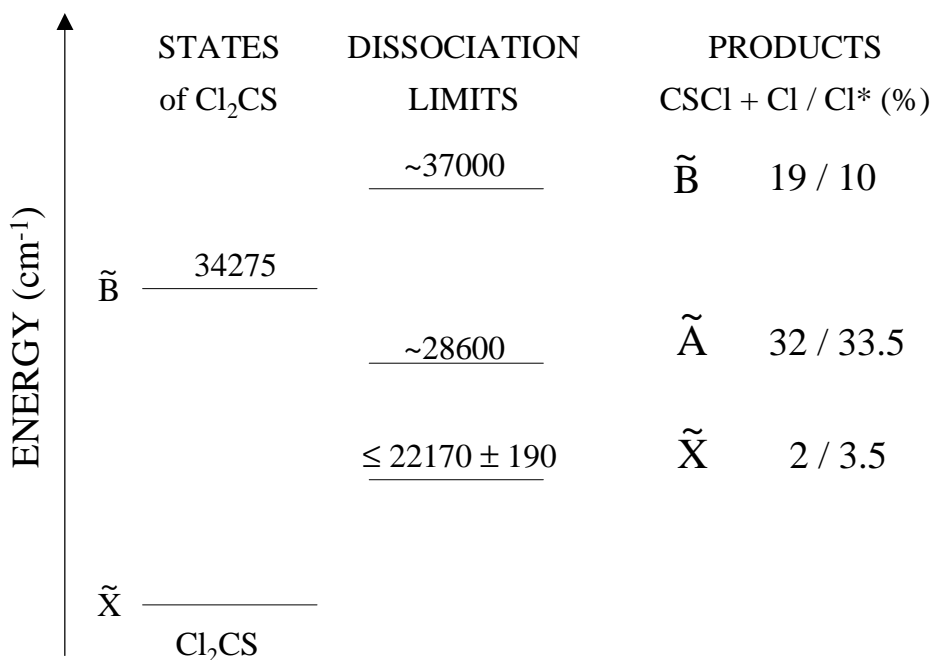


Figure 4.4: Energy level diagram for CSCI₂ and its dissociation products taken from Hachey et al.¹¹ The energy levels are given relative to the ground state \tilde{X} of CSCI₂. The observed correlation to the ground or excited state of chlorine in the products are added.

The overall contributions of the CSCI \tilde{X} , \tilde{A} , and \tilde{B} states can be determined by the three Gaussians which are fitted to the IED taking the calculation by Hachey et al.¹⁶ into account. Integrating the area under the Gaussian profiles yield the ratio of 1:13:6 for CSCI(\tilde{X}):CSCI(\tilde{A}):CSCI(\tilde{B}), summed over both chlorine atom spin-orbit states. Clearly, the generation of CSCI(\tilde{X}) is only a minor channel. In the case of ground state Cl, the states \tilde{X} , \tilde{A} , and \tilde{B} of CSCI contribute to 1:15:9, respectively. Cl in its ground state is predominantly released with a CSCI partner fragment with high internal energy up to the energetic limit. In the case of spin-orbit excited Cl* the contributions of the states \tilde{X} , \tilde{A} , and \tilde{B} of CSCI are 1:9.5:2.8, respectively.

The observed contribution of the different CSCI states allows to speculate that CSCI₂ would decay into three fragments releasing two slow ground state Cl, if the three-body threshold will be passed by increasing the photolysis energy. With respect to Cl* the shape of the contribution (lower panel of Fig. 4.3) suggests that Cl* would be released as a minor product if the three-body decay channel \tilde{X} is energetically allowed. This view is further supported by the CSCI state-specific $P(\text{Cl}^*)/P(\text{Cl})$ branching ratios which drop from 1.6 for the \tilde{X} to 1.2 for the \tilde{A} states, and to 0.6 for the \tilde{B} state.

In addition, due to the geometry change by exciting CSCI₂ a significant rotational excitation of the electronically excited CSCI radical seems likely, with a tendency to realize a three-body decay as soon as the respective threshold energy is surpassed. A large internal fragment excitation favoring a three-body decay upon transgressing the three-body threshold was observed for COCl₂ and COFCl upon excitation in the first absorption bands associated with the ¹A₂ state. The same behavior is also found upon excitation of the ¹A₁ band of CSCI₂. Whereas different electronic excitations are involved they have the same excited π^*_{CS} molecular orbital in common. The observations on CSCI₂ in conjunction with the observations on COCl₂ and COFCl therefore suggest that the tendency towards exhibiting an early three-body decay is linked to the excitation of a π^* electron in the double bond on the far side of the molecule, i.e. opposite to the bonds that are to be broken. A subsequent rearrangement of the energy initially deposited in the CS bond channels a significant portion into the dissociation coordinate of the intermediate CSCI fragment leading to its eventual unimolecular decay. In agreement with the above, in the vibrationally mediated dissociation of CHFCl₂⁴⁰ and CH₃CFCl₂⁴¹ vibrational energy initially

deposited in the CH vibrational degrees of freedom is redistributed to all degrees of freedom of the intermediate after departure of the first Cl fragment. Due to the larger number of degrees of freedom not associated with the dissociation coordinate, the contribution of three-body decay was small for CHFCI₂ and almost absent for CH₃CFCl₂. This supports our view that the excitation of the far double bond tends to produce a sequential or at least a slow concerted three-body decay in small polyatomic molecules such as carbonyl halides and related species.

4.4 Conclusions

The photodissociation of CSCI₂ at 235 nm was studied by a novel REMPI-TOF 3D imaging technique. The 3D velocity distribution of excited state Cl* and ground state Cl and the respective anisotropy parameters β as a function of the recoil velocity were measured. The β parameter was found to be essentially velocity independent with an averaged value of 0.03 ± 0.06 .

The kinetic energy distribution of the ground state Cl is bimodal releasing Cl mainly with low kinetic energy, whereas the KED of the excited state Cl* is broad showing no preference for very low kinetic energies.

The kinetic energy distributions of Cl and Cl* include the information of the corresponding states of the CSCI partner fragment. It was found that the main partner of both Cl and Cl* is CSCI in the excited state \tilde{A} and \tilde{B} , and the generation of CSCI(\tilde{X}) is only a minor channel. Considering the electronical energy E_{el} of 77 kJ/mol for the \tilde{A} state and 178 kJ/mol for the \tilde{B} state of the CSCI, an internal energy release of 75 kJ/mol for CSCI(\tilde{X}), 98 kJ/mol for CSCI(\tilde{A}), and 47 kJ/mol for CSCI(\tilde{B}) is evaluated if the Cl partner is generated in its ground state. For the Cl* channel respective values of 57, 77, and 23 kJ/mol are obtained. By taking the spin-orbit branching ratio of $P(\text{Cl}^*)/[P(\text{Cl})+P(\text{Cl}^*)]$ of 0.47 into account, the absolute values of the contribution of \tilde{X} , \tilde{A} , and \tilde{B} states are 5.5 ± 0.5 %, 65.5 ± 5 %, and 29.0 ± 3 %, respectively.

The energy release $E_T/(E_{av} - E_{el})$ was found to be 0.69 ± 0.04 , 0.41 ± 0.03 , and 0.28 ± 0.03 for ground state Cl and CSCI(\tilde{X}), CSCI(\tilde{A}), and CSCI(\tilde{B}), respectively and 0.75 ± 0.05 , 0.50 ± 0.03 , and 0.57 ± 0.04 for spin excited Cl* and CSCI(\tilde{X}), CSCI(\tilde{A}), and CSCI(\tilde{B}). A significant rotational excitation of the electronically excited CSCI radical seems likely followed by a three-body decay as soon as the respective threshold is surpassed.

4.5 Acknowledgement

These studies were supported by the Fonds der Chemischen Industrie, the Alexander von Humboldt Stiftung, and the German-Israeli-Foundation (GIF). Financial support by the Deutsche Forschungsgemeinschaft is gratefully acknowledged.

-
- ¹ A. Chichinin, T. Einfeld, C. Maul, and K.-H. Gericke, *Rev. Sci. Instr.* **73**, N4, xxx (2002).
 - ² T. Einfeld, A. Chichinin, C. Maul, and K.-H. Gericke, in preparation.
 - ³ T. Einfeld, A. Chichinin, C. Maul, and K.-H. Gericke, *J. Chem. Phys.* **116**, 2803 (2002).
 - ⁴ M. Kawasaki, K. Kasatani, H. Sato, H. Shinohara, N. Nishi, H. Ohtoshi, and I. Tanaka, *Chem. Phys.* **91**, 285 (1984); G. Baum, C. S. Effenhauser, P. Felder, and J. R. Huber, *J. Phys. Chem.* **96**, 756 (1992); M. Kawasaki, K. Suto, Y. Sato, Y. Matsumi, and R. Bersohn, *J. Phys. Chem.* **100**, 19853 (1996); C. Maul and K.-H. Gericke, *J. Phys. Chem. A* **104**, 2531 (2000).
 - ⁵ C. Maul, T. Haas, and K.-H. Gericke, *J. Chem. Phys.* **102**, 3238 (1995); C. Maul, T. Haas, and K.-H. Gericke, *J. Phys. Chem. A* **101**, 6619 (1997).
 - ⁶ A. Maciejewski and R. P. Steer, *Chem. Rev.* **93**, 67 (1993).
 - ⁷ D. J. Clouthier and D. C. Moule, *Top. Curr. Chem.* **150**, 167 (1989).
 - ⁸ B. Simard, V. J. MacKenzie, P. A. Hackett, and R. P. Steer, *Can. J. Chem.* **72**, 745 (1994).
 - ⁹ M. Ludwiczak, D. R. Latimer, and R. P. Steer, *J. Mol. Spectrosc.* **147**, 414 (1991).
 - ¹⁰ A. Maciejewski, M. Szymanski, and R. P. Steer, *Chem. Phys.* **165**, 101 (1992).
 - ¹¹ K. J. Falk, S. E. Sveinson, and R. P. Steer, *Chem. Phys. Lett.* **163**, 490 (1989).
 - ¹² M. Szymanski, S. E. Sveinson, and R. P. Steer, *J. Phys. Chem.* **95**, 5159 (1991).
 - ¹³ A. Maciejewski, M. Szymanski, and R. P. Steer, *J. Chem. Soc. Faraday Trans.* **89**, 3251 (1993).
 - ¹⁴ H. Okabe, *J. Chem. Phys.* **79**, 175 (1983).
 - ¹⁵ G. S. Ondrey and R. Bersohn, *J. Chem. Phys.* **79** (1), 175 (1983).
 - ¹⁶ A. Hachey, F. Grein, and R. P. Steer, *Can. J. Chem.* **71**, 112 (1993).
 - ¹⁷ J. H. Carpenter, D. F. Rimmer, J. G. Smith, and D. H. Whiffen, *J. Chem. Soc. Faraday Trans. 2*, **71**, 1752 (1975).

- ¹⁸ D. Chadwick, *Can. J. Chem.* **50**, 737 (1972).
- ¹⁹ E. R. Farnworth and G. W. King, *J. Mol. Spectrosc.* **57**, 215 (1975).
- ²⁰ R. Bigwood, B. Milam, and M. Gruebele, *Chem. Phys. Lett.* **287**, 333-341 (1998).
- ²¹ D. C. Moule and C. R. Subramaniam, *J. Mol. Spectrosc.* **48**, 336 (1973).
- ²² T. Oka, A. R. Knight, and R. P. Steer, *J. Chem. Phys.* **63**, 2414 (1975); D. J. Clouthier, P. A. Hackett, A. R. Knight, and R. P. Steer, *J. Photochem.* **17**, 319 (1981); D. J. Clouthier, A. R. Knight, R. P. Steer, and P. A. Hackett, *J. Chem. Phys.* **72**, 1560 (1980); D. M. Brenner, M. N. Spencer, and J. I. Steinfeld, *J. Chem. Phys.* **78**, 136 (1983).
- ²³ J. R. McDonalds, L. E. Brus, *Chem. Phys. Lett.* **16**, 587 (1972); S. Z. Levine, A. R. Knight, and R. P. Steer, *Chem. Phys. Lett.* **29**, 73 (1974).
- ²⁴ J. C. D. Brand, J. L. Hardwick, and K. E. Teo, *J. Mol. Spectrosc.* **57**, 215 (1975).
- ²⁵ C. Maul and K.-H. Gericke, *Int. Rev. Phys. Chem.* **16**, 1 (1997).
- ²⁶ C. Maul, C. Dietrich, T. Haas, and K.-H. Gericke, *Phys. Chem. Chem. Phys.* **1**, 1441 (1999).
- ²⁷ G. E. Busch and K. R. Wilson, *J. Chem. Phys.* **56**, 3638 (1972).
- ²⁸ W. T. Chan and J. D. Goddard, *Chem. Phys. Lett.* **173**, 139 (1990).
- ²⁹ S. E. Sobottka and M. B. Williams, *IEEE Trans. Nucl. Science* **35**, 348 (1988).
- ³⁰ O. Jagutzki, V. Mergel, K. Ullmann-Pfleger, L. Spielberger, U. Meyer, R. Dörner, and H. Schmidt-Böcking, *Fast position and time-resolved read-out of micro-channel plates with the delay-line technique for single particle and photon detection*, proceedings in Imaging Spectroscopy IV, 322 San Diego, California (1998).
- ³¹ M. Lampton, O. Siegmund, and R. Raffanti, *Rev. Sci. Instr.* **58**, 2298 (1987).
- ³² J. Danielak, U. Domin, R. Kepa, M. Rytel, and M. Zachwieja, *J. Mol. Spect.* **181**, 394 (1997).
- ³³ R. H. Judge and D. C. Moule, *J. Mol. Spectrosc.* **80**, 363 (1980).
- ³⁴ D. A. Prinslow and P. B. Armentrout, *J. Chem. Phys.* **94**, 3563 (1991).
- ³⁵ R. M. Joshi, *J. Macromol. Sci. Chem.* **A 13** (7), 1015 (1979).
- ³⁶ J. Li and R. P. Steer, *Can. J. Chem.* **73**, 131 (1995).
- ³⁷ P. M. Regan, S. R. Langfold, D. Ascenzi, P. A. Cook, A. J. Orr-Ewing, and M. N. R. Ashfold, *Phys. Chem. Chem. Phys.* **1**, 3247 (1999).
- ³⁸ H. Okabe, *J. Chem. Phys.* **53**, 3507 (1970); H. Okabe, *Photochemistry of Small Molecules* (Wiley-Interscience, New York, 1978).
- ³⁹ R. Schinke, *Photodissociation Dynamics*, Cambridge Monographs on Atoms, Molecular and Chemical Physics 1 (Cambridge University Press, 1993).
- ⁴⁰ X. Chen, R. Marom, S. Rosenwaks, I. Bar, T. Einfeld, C. Maul, and K.-H. Gericke, *J. Chem. Phys.* **114**, 9033 (2001).
- ⁴¹ T. Einfeld, C. Maul, K.-H. Gericke, R. Marom, S. Rosenwaks, and I. Bar, *J. Chem. Phys.* **115**, 6418 (2001).